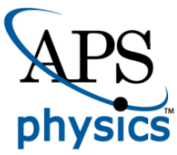

Intrinsic Two-Dimensional Ferroelectricity with Dipole Locking

Jun Xiao, Hanyu Zhu, Ying Wang, Wei Feng, Yunxia Hu, Arvind Dasgupta, Yimo Han, Yuan Wang, David A. Muller, Lane W. Martin, PingAn Hu, and Xiang Zhang

Phys. Rev. Lett. **120**, 227601 — Published 31 May 2018

DOI: 10.1103/PhysRevLett.120.227601

Intrinsic two-dimensional ferroelectricity with dipole locking

Jun Xiao,[1†] Hanyu Zhu,[1†] Ying Wang,[1†] Wei Feng,[2] Yunxia Hu,[2] Arvind Dasgupta,[3] Yimo Han,[4] Yuan Wang,[1] David A. Muller,[4,5] Lane W. Martin,[3,6] PingAn Hu,[2] Xiang Zhang[1,6]*

[1] NSF Nanoscale Science and Engineering Center (NSEC), University of California, Berkeley, California 94720, USA

[2] School of Materials Science and Engineering, Harbin Institute of Technology, Harbin 150080, P. R. China

[3]Department of Materials Science and Engineering, University of California, Berkeley, California 94720, USA

[4]Department of Applied and Engineering Physics, Cornell University, Ithaca, NY 14853, USA

[5]Kavli Institute at Cornell for Nanoscale Science, Ithaca, NY 14853, USA

[6]Materials Sciences Division, Lawrence Berkeley National Laboratory, 1 Cyclotron Road, Berkeley, California, USA

[†] These authors contributed equally to this work.

*Correspondence author. E-mail: xiang@berkeley.edu

Abstract

Out-of-plane ferroelectricity with a high transition temperature in ultrathin films is important for the exploration of new domain physics and scaling down of memory devices. However, depolarizing electrostatic fields and interfacial chemical bonds can destroy this

long-range polar order at two-dimensional (2D) limit. Here we report the discovery of the locking between out-of-plane dipoles and in-plane lattice asymmetry in atomically thin In_2Se_3 crystals, a new stabilization mechanism leading to our observation of intrinsic 2D out-of-plane ferroelectricity. Through second harmonic generation (SHG) spectroscopy and piezoresponse force microscopy (PFM), we found switching of out-of-plane electric polarization requires simultaneous flip of nonlinear optical polarization that corresponds to the inversion of in-plane lattice orientation. The polar order shows a very high transition temperature (~700 K) without the assistance of extrinsic screening. This finding of intrinsic 2D ferroelectricity resulting from dipole locking opens up possibilities to explore 2D multiferroic physics and develop ultrahigh density memory devices.

Ferroelectric ordering dictates electrically switchable macroscopic polarization, arising from spontaneous alignment of electric dipoles [1,2]. Such collective phase reveals fundamental interplay between crystal symmetry and quasiparticle interactions [3,4]. The development of ferroelectric materials such as barium titanate ($BaTiO_3$) was also prompted by applications like electromechanical actuators and storage devices [5]. However, the strength of polarization and transition temperature drop as ferroelectric films scale down due to the reduced long-range Coulomb coupling and enhanced depolarization field, and ferroelectricity disappears below a critical thickness around several to tens of nanometers [1,6–8]. In addition, interfacial bonding related strain and chemical environment can also deteriorate thin film ferroelectricity [9–11]. In contrast, the emerging van der Waals layered materials have strong intralayer chemical bonds but weak interlayer interactions, and thus could provide a pathway to eliminate the role of interfacial defects and strain. With the presence of this strong anisotropy, 2D layered materials may go beyond such limitations and are unique platforms to study fundamental electronic and structural ordering in two dimensions [12–14]. Furthermore, the ferroelectric switching allows the control of asymmetry-induced properties in 2D layered materials such as spin-orbit coupling, valley degree of freedom and anisotropic transport [15,16].

Here we experimentally demonstrate intrinsic out-of-plane 2D ferroelectric ordering in atomically thin In_2Se_3 crystals with thickness down to 3 nm, and verify the unique polarization locking mechanism in accordance to the theoretical prediction [17]. Each In_2Se_3 layer contains five triangular atomic lattices stacked in the sequence of Se-In-Se-In-Se through covalent bonds and belongs to *R3m* space group (No. 160). The asymmetric position of Se atom in the middle spontaneously breaks the centrosymmetry, providing two energetically-degenerate states with opposite out-of-plane electric polarization and in-plane asymmetry with reverse second-order nonlinear polarization (Fig. 1a and b). The stabilization of ferroelectricity is achieved primarily through the out-of-plane and in-plane polarization locking enforced by unique covalent bond configuration of In_2Se_3 crystal, instead of long-range Coulomb interaction in conventional ferroelectric materials [18]. To erase or even flip the out-of-plane electrical polarization, the middle Se atom must also move laterally (~ 100 pm) accompanied by the In-Se covalent bonds breaking and forming [17]. It is fundamentally distinct from traditional ferroelectric switching wherein small uniaxial atomic distortions (~ 10 pm) occur without bond breaking in, for example, perovskite oxides or via molecular chain rotation in PVDF [19]. Such additional in-plane atomic movement enforced by locking provides strong resistance for out-of-plane polarization against depolarization field. Accordingly, the calculated domain wall energy is also several times to more than one order of magnitude larger than that in perovskite oxides such as $PbTiO_3$ and $BaTiO_3$ [17,20,21]. These features also distinguish the ferroelectricity in In_2Se_3 from recent reports on atomically thin SnTe and $CuInP_2S_6$ [22,23], whose polarization only involves either pure in-plane or out-of-plane atomic distortion without breaking of covalent bonds. As a consequence, SnTe cannot exhibit out-of-plane polar order, while the ferroelectricity in $CuInP_2S_6$ does not exist below 50 nm in the absence of extrinsic electronic screening by a conductive substrate.

We prepared atomically thin membranes of In_2Se_3 by both exfoliation and van der Waals epitaxial growth (Supplementary Material section I) [24,25]. Their thickness was then determined by atomic force microscopy, and the single layer step height is 1 nm (Supplementary Material section II and Fig. S1). To verify the presence of in-plane and out-of-plane asymmetry, which is

the prerequisite for ferroelectricity, we performed SHG studies with normal and oblique incidence at ambient conditions (Supplementary Material section I and III, Fig. S2). First, the SHG signal from a trilayer sample on insulating mica substrate can be observed under normal incidence (Fig. S3a), which indicates inversion symmetry breaking with the presence of in-plane nonlinear optical polarization. The polarization-resolved SHG shows a six-fold intensity pattern when the normal incident excitation and detection polarization are rotated collinearly (Fig. 1c). Given the coordinate axes depicted in Fig. 1b, the responsible tensor components for the SHG signal in Fig. 1c are χ_{xxx}, χ_{xyy}, χ_{yxy} and χ_{yyx} according to the R_{3m} space group. Based on detailed symmetry analysis (Supplementary Material section III) [26,27], the maximum of each lobe corresponds to the In-Se bond armchair direction. Although this three-fold rotational symmetry prohibits in-plane electric dipole polarization, it gives an effective in-plane second-order optical dipole emission due to inversion symmetry breaking [28]. Next, we used angle-resolved polarization-selective SHG measurements to observe the out-of-plane dipole [29]. By rotating the crystal to make the In-Se bond direction perpendicular to both the incident and detecting polarization direction, the SHG induced by the in-plane dipole is made extinct. Then the vertical electric field in a tilted beam drives the out-of-plane dipole and gives rise to a SHG signal (Fig. S3b). Figure 1d shows the incident angle dependent SHG from the out-of-plane dipole in the same trilayer sample, normalized with collection efficiency. As the tilt angle increases, SHG intensity increases as the z-component of the optic electrical field becomes stronger and is symmetric for positive and negative tilt angle. This observation confirmed the presence of an out-of-plane asymmetry in the In_2Se_3 ultrathin crystals, which is the prerequisite for 2D out-of-plane ferroelectricity. The ratio between in-plane and out-of-plane second-order susceptibility is 13.6:1 at 1080 nm pump (Supplementary Material section III), consistent with the theoretical estimation that the static in-plane dipole is more than one order of magnitude larger than the out-of-plane dipole [17]. An annular dark-field scanning transmission electron microscopy (ADF-STEM) cross-section image of a multilayer In_2Se_3 also confirms the asymmetric ferroelectric crystal structure as predicted (Supplementary Material section IV and Fig. S4). Meanwhile, the samples with strong SHG signal display the same Raman characteristic peaks (Supplementary Material section V and Fig. S5), as reported for α-phase In_2Se_3 [24].

In addition to the presence of dipoles, SHG and complementary PFM mapping of the trilayer at room temperature reveals domains and domain boundaries as shown in Fig. 2. The region with stronger SHG displays larger piezoresponse, while the region with weaker SHG shows smaller piezoresponse amplitude. The correlation indicates that the as-grown sample contains domains with different net dipole strength. We verified that the dipole strength difference does not come from composition inhomogeneity, because both regions give the same Raman spectra (Fig.S6a), meaning they have the same crystal phase. Therefore, we postulate that for as-grown sample, some regions are well aligned along one polarization, while other regions may partially include lattice configuration with opposite polarization and reduce the average nonlinear optical response. Similar intensity variation has also been observed for SHG generated by out-of-plane dipole (Fig. S6b). In addition, in the SHG image we observed dark lines within the area that has uniform optical contrast (Fig. 2a). By superimposing these dark lines onto the piezoresponse and the phase mapping (blue curves in Fig. 2b, c), we found that they always occur at the boundaries of two 180-degree domains with comparable piezoresponse and SHG amplitude. The consistency proves that they result from destructive interference between the optical fields from adjacent domains with opposite polarizations (Supplementary Material section VII) [30]. On the other hand, for the boundary between a domain with large positive piezoresponse and a domain with small negative piezoresponse, SHG dark lines are shadowed due to the imperfect optical destructive interference.

Beyond the presence of polar structures with opposite spontaneous polarizations, we also demonstrated the switch of the polarization by applying electric field. Indeed, for ultrathin ferroelectric In_2Se_3, large out-of-plane field (~1V/nm) is predicted to flip the out-of-plane polar order. In the following, we demonstrated such polarization switching with vertical electric bias at room temperature. The sample was prepared by transferring the as-grown In_2Se_3 flakes onto strontium ruthenium oxide ($SrRuO_3$) thin film deposited on a (001)-oriented strontium titanate ($SrTiO_3$) substrate, which served as the back electrode. The electric field was applied through a conductive tungsten carbide probe with radius of 20 nm, and then the polarization switching was observed separately through inverse piezoelectric effect by resonance-enhanced piezoresponse force microscopy (Supplementary Material section VIII). Figure 3a shows the single-point off-field hysteresis loop of the piezoresponse as a function of poling electric field for a trilayer flake.

With small probe voltage of 0.5 V, the coercive field of this piezoresponse loop is about 2-3 V over the 3-nm thickness, comparable to the theoretical prediction. Such observed large coercivity confirms the large energy barrier between the two polarization states, which is necessary to combat the depolarization field at the 2D limit. As the probe voltage increases to 1.5 V close to the coercive field, the loop collapses in both amplitude and width. This is a clear signature of field-switchable electromechanical deformation expected from ferroelectricity in In_2Se_3, and distinguished from the electrostatic force-induced artifacts from charging in non-ferroelectric materials [31]. Based on the obtained coercive field of 3-nm-thick the trilayer, we further observed areal ferroelectric domain reversal by scanning the probe with constant bias. Both positive and negative piezoresponse domains were written onto the trilayer sample as shown in Figure 3b. The pattern remained stable in ambient conditions for at least three days when it was probed again. It should be noted that although other contributions (*e.g.,* injected charge, chemical changes, diffusion of species, etc.) can give rise to PFM contrast [32,33], the long-term stability of this signal suggests a link with the structural change and not one of these other spurious effects. In particular, we exclude charging effect as the source of the electromechanical response, which should quickly dissipate for ultrathin semiconducting film on conductive substrate.

More strikingly, the unique polarization locking relationship in In_2Se_3 crystal structure requires that the in-plane atomic motion locked with the out-of-plane polarization switching and enables control in-plane asymmetry by out-of-plane electric fields. To demonstrate such control, we firstly selected one region of a trilayer In_2Se_3 sample on the $SrRuO_3/SrTiO_3$ (001) substrate showing strong SHG under normal incidence originating from in-plane dipoles (Fig. 3c). Next, a square region was scanned by a negatively biased probe and enclosed by dashed line (Fig. 3c). The “writing” condition of negative electrical bias is the same as that applied in Fig. 3b, where the domain flipping at a single point was achieved during the hysteresis loop measurement. After the “writing” process, the orientation of the in-plane dipole was probed by SHG under normal incidence. Compared with the mapping before patterning, it showed nearly uniform SHG intensity distribution outside the “writing” region as well as nearly uniform SHG intensity inside after reversal poling (Fig. 3d). Notably, we also observed clear dark lines with low SHG intensity exactly overlapping with the boundaries defined by the PFM writing pattern, evidencing destructive optical interference because of the reversal of the in-plane nonlinear optical

polarization and corresponding in-plane lattice asymmetry by the out-of-plane electric field patterning. Such observations further prove the strict locking between in-plane and out-of-plane dipoles and allows electrical switching of in-plane crystalline symmetry by vertical electrical field.

Finally, we observed evidence of a temperature-induced phase transition in the ultrathin In_2Se_3 around 700 K by temperature-dependent SHG (Fig. 4). In a normal ferroelectric, increasing the temperature produces strong thermal fluctuations which act to destabilize the spontaneous polarization and drive the material into a high-temperature, high-symmetry structure possessing inversion symmetry. Similar effects were observed for a four-layer In_2Se_3 crystal transferred on a SiO_2/Si substrate. we first observed gradual SHG intensity decrease as a function of temperature over a broad range. The slow amplitude reduction of the SHG signal again confirms the robustness of the polar order. Starting at ~600 K, a sharp SHG intensity drop occurs, indicating the rapid disappearance of spontaneous polarization and the potential transition to a centrosymmetric phase. The observed high transition temperature is attributed to the energy difference between ferroelectric and high-temperature phases and the large kinetic transition barrier involving both in-plane and out-of-plane bond reconfiguration.

The realization of intrinsic out-of-plane ferroelectricity in ultrathin crystal is important for exploration on novel phase ordering with quantum confinement and enhanced quasiparticle interactions [34,35], which is absent in the thick films. Unconventional phase competition is expected when the depolarization field becomes significant in ultrathin film with a thickness of several nanometers. Also, the large mechanical and electrical tunability of atomically thin layered materials [36–38], may not only reveal rich phase transition physics but enable versatile ultrathin ferroelectric devices. Although ferroelectricity in In_2Se_3 flakes with thickness of a few tens of nanometers was reported recently [34], it is far away from atomically thin limit for exploration on above unique physics and applications. On the contrary, our study shows robust out-of-plane ferroelectricity in atomically thin In_2Se_3 (~ 3 nm) with an ultra-high transition temperature (~700 K). Meanwhile, our first experimental confirmation of the strict locking between out-of-plane dipoles and in-plane covalent lattice asymmetry, a completely new

mechanism to stabilize the 2D intrinsic ferroelectricity, provides a new degree of freedom to control structural and electronic ordering in layered materials and multiferroic heterostructures.

In conclusion, we demonstrated optical and electromechanical evidences in atomically thin In_2Se_3 crystal that satisfy the criteria for ferroelectric materials [1,39,40]: spontaneous polar ordering in the absence of an external electrical field probed by SHG; switching of such polarization by an electrical field observed by both PFM and SHG. Such ferroelectricity is intrinsically stable against depolarization field even on dielectric substrates with little screening, protected by dipole locking due to its unique covalent bond configuration. Furthermore, the ferroelectric phase of In_2Se_3 has high transition temperature ~700 K. This discovery features new polarization switching mechanism involving covalent bond reconstruction and provides a unique platform to explore 2D ferroelectric physics and establish novel 2D optoelectronic devices based on polarization locking relationship.

Acknowledgement

We acknowledge technical support from Ed Wong on high-T vacuum chamber preparation. J.X., H.Z., Y.W., Y.W., X.Z. acknowledge the support from National Science Foundation (EFMA-1542741). W.F., Y.H. and P.H. were supported by the National Natural Science Foundation of China (NSFC, No. 61390502 and 61505033). A.D. acknowledges support from the National Science Foundation under grant DMR-1708615. L.W.M. acknowledges support from the Army Research Office under grant W911NF-14-1-0104. Y.H. and D.A.M. were supported by the Cornell Center for Materials Research with funding from the NSF MRSEC program (DMR-1719875).

Reference

[1] M. E. Lines and A. M. Glass, *Principles and Applications of Ferroelectrics and Related Materials* (Oxford University Press, 2001).

[2] M. Dawber, K. M. Rabe, and J. F. Scott, Rev. Mod. Phys. **77**, 1083 (2005).

[3] T. Egami, S. Ishihara, and M. Tachiki, Science **261**, 1307 (1993).

[4] A. K. Yadav, C. T. Nelson, S. L. Hsu, Z. Hong, J. D. Clarkson, C. M. Schlepütz, A. R. Damodaran, P. Shafer, E. Arenholz, L. R. Dedon, D. Chen, A. Vishwanath, A. M. Minor, L. Q. Chen, J. F. Scott, L. W. Martin, and R. Ramesh, Nature **530**, 198 (2016).

[5] J. F. Scott, Science **315**, 954 (2007).

[6] E. A. Eliseev, S. V. Kalinin, and A. N. Morozovska, J. Appl. Phys. **117**, 034102 (2015).

[7] C. H. Ahn, K. M. Rabe, and J.-M. J.-M. Triscone, Science **303**, 488 (2004).

[8] J. Junquera and P. Ghosez, Nature **422**, 506 (2003).

[9] Y. Wang, M. K. Niranjan, K. Janicka, J. P. Velev, M. Y. Zhuravlev, S. S. Jaswal, and E. Y. Tsymbal, Phys. Rev. B **82**, 094114(2010).

[10] C. G. Duan, R. F. Sabirianov, W. N. Mei, S. S. Jaswal, and E. Y. Tsymbal, Nano Lett. **6**, 483 (2006).

[11] C.-L. Jia, V. Nagarajan, J.-Q. He, L. Houben, T. Zhao, R. Ramesh, K. Urban, and R. Waser, Nat. Mater. **6**, 64 (2007).

[12] X. Xi, Z. Wang, W. Zhao, J.-H. Park, K. T. Law, H. Berger, L. Forró, J. Shan, and K. F. Mak, Nat. Phys. **12**, 139 (2015).

[13] Y. Saito, Y. Kasahara, J. Ye, Y. Iwasa, and T. Nojima, Science **350**, 409 (2015).

[14] Y. Yu, F. Yang, X. F. Lu, Y. J. Yan, H. ChoYong, L. Ma, X. Niu, S. Kim, Y.-W. Son, D. Feng, S. Li, S.-W. Cheong, X. H. Chen, and Y. Zhang, Nat Nano **10**, 270 (2015).

[15] K. F. Mak, K. He, J. Shan, and T. F. Heinz, Nat. Nanotechnol. **7**, 494 (2012).

[16] F. Xia, H. Wang, and Y. Jia, Nat. Commun. **5**, 4458 (2014).

[17] W. Ding, J. Zhu, Z. Wang, Y. Gao, D. Xiao, Y. Gu, Z. Zhang, and W. Zhu, Nat. Commun. **8**, 14956 (2017).

[18] G. A. Samara, T. Sakudo, and K. Yoshimitsu, Phys. Rev. Lett. **35**, 1767 (1975).

[19] W. J. Hu, D.-M. Juo, L. You, J. Wang, Y.-C. Chen, Y.-H. Chu, and T. Wu, Sci. Rep. **4**, 4772 (2014).

[20] M. Li, Y. Gu, Y. Wang, L. Q. Chen, and W. Duan, Phys. Rev. B **90**, 054106 (2014).

[21] B. Meyer and D. Vanderbilt, Phys. Rev. B **65**, 104111 (2002).

[22] K. Chang, L. Junwei, L. Haicheng, N. Wang, K. Zhao, A. Zhang, F. Jin, Y. Zhong, X. Hu, W. Duan, Q. Zhang, L. Fu, Q.-K. Xue, X. Chen, and S.-H. Ji, Science **353**, 274 (2016).

[23] F. Liu, L. You, K. L. Seyler, X. Li, P. Yu, J. Lin, X. Wang, J. Zhou, H. Wang, H. He, S. T. Pantelides, W. Zhou, P. Sharma, X. Xu, P. M. Ajayan, J. Wang, and Z. Liu, Nat. Commun. **7**, 12357 (2016).

[24] X. Tao and Y. Gu, Nano Lett. **13**, 3501 (2013).

[25] W. Feng, W. Zheng, F. Gao, X. Chen, G. Liu, T. Hasan, W. Cao, and P. Hu, Chem. Mater. **28**, 4278 (2016).

[26] L. M. Malard, T. V. Alencar, A. P. M. Barboza, K. F. Mak, and A. M. De Paula, Phys. Rev. B **87**, 201401 (2013).

[27] Y. R. Shen, *Principles of Nonlinear Optics* (John Wiley & Sons, Inc., 2002).

[28] Y. Li, Y. Rao, K. F. Mak, Y. You, S. Wang, C. R. Dean, and T. F. Heinz, Nano Lett. **13**, 3329 (2013).

[29] A.-Y. Lu, H. Zhu, J. Xiao, C.-P. Chuu, Y. Han, M.-H. Chiu, C.-C. Cheng, C.-W. Yang, K.-H. Wei, Y. Yang, Y. Wang, D. Sokaras, D. Nordlund, P. Yang, D. A. Muller, M.-Y. Chou, X. Zhang, and L.-J. Li, Nat. Nanotechnol. **12**, 744 (2017).

[30] S. A. Denev, T. T. A. Lummen, E. Barnes, A. Kumar, and V. Gopalan, J. Am. Ceram. Soc. **94**, 2699 (2011).

[31] N. Balke, P. Maksymovych, S. Jesse, A. Herklotz, A. Tselev, C. B. Eom, I. I. Kravchenko, P. Yu, and S. V. Kalinin, ACS Nano **9**, 6484 (2015).

[32] S. Hong, J. Woo, H. Shin, J. U. Jeon, Y. E. Pak, E. L. Colla, N. Setter, E. Kim, and K. No, J. Appl. Phys. **89**, 1377 (2001).

[33] N. Balke, S. Jesse, Q. Li, P. Maksymovych, M. Baris Okatan, E. Strelcov, A. Tselev, and S. V. Kalinin, J. Appl. Phys. **118**, 072013 (2015).

[34] Z. Ye, T. Cao, K. O'Brien, H. Zhu, X. Yin, Y. Wang, S. G. Louie, and X. Zhang, Nature **513**, 214 (2014).

[35] A. Chernikov, T. C. Berkelbach, H. M. Hill, A. Rigosi, Y. Li, O. B. Aslan, D. R. Reichman, M. S. Hybertsen, and T. F. Heinz, Phys. Rev. Lett. **113**, 076802 (2014).

[36] K. F. Mak, K. He, C. Lee, G. H. Lee, J. Hone, T. F. Heinz, and J. Shan, Nat. Mater. **12**, 207 (2013).

[37] J. T. Ye, Y. J. Zhang, R. Akashi, M. S. Bahramy, R. Arita, and Y. Iwasa, Science **338**, 1193 (2012).

[38] D. Akinwande, N. Petrone, and J. Hone, Nat. Commun. **5**, 5678 (2014).

[39] K. M. Rabe, C. H. Ahn, J. M.-M. Triscone, M. Dawber, and C. Lichtensteiger, *Physics of Ferroelectrics* (Springer, 2007).

[40] C. Kittel, *Introduction to Solid State Physics* (John Wiley & Sons, Inc., 2004).

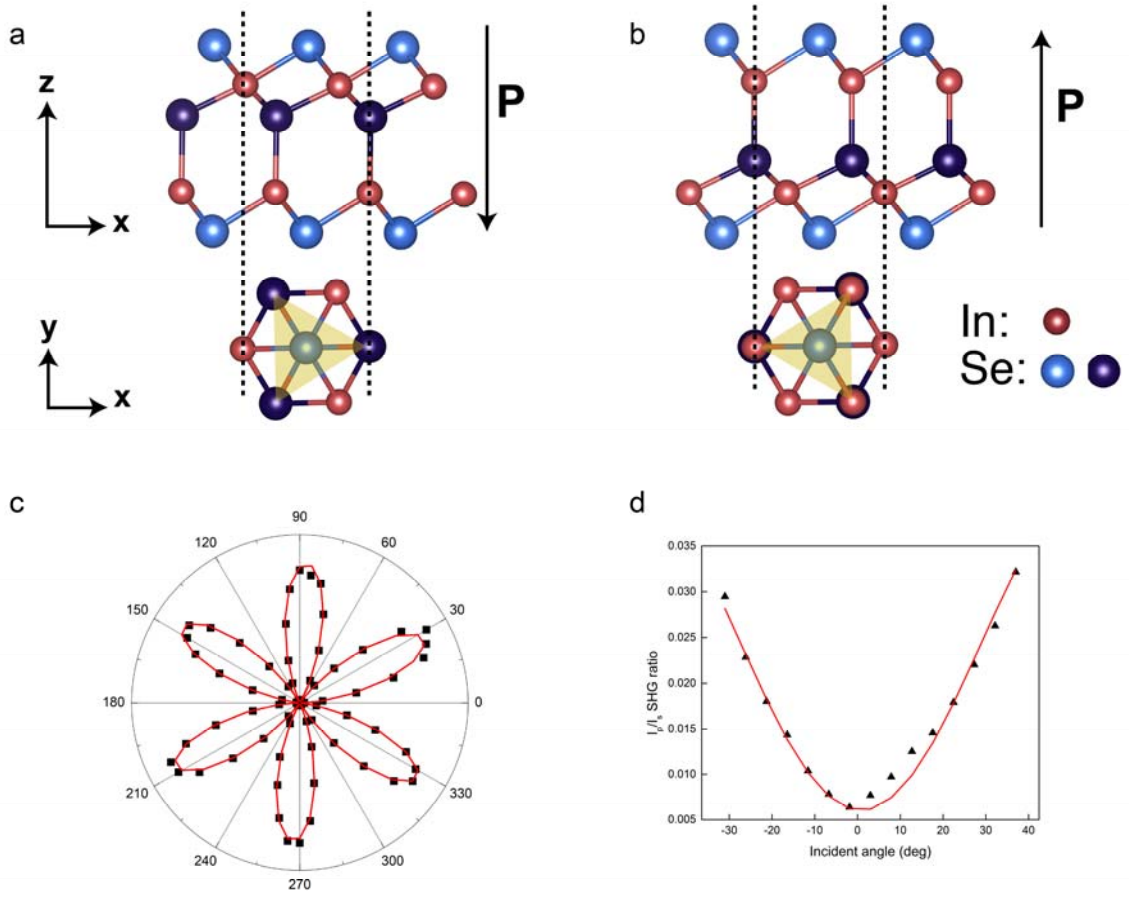

Figure 1 | Characterization of 2D In_2Se_3. a, b, Side and top view of two energy-degenerate ferroelectric In_2Se_3 structures. Single quintuple layer consists of covalently bonded indium and selenium triangular lattices. The crystal belongs to *R3m* space group (No. 160). The polarization

flipping requires locked out-of-plane and in-plane motion of middle Se atom (purple ball) accompanied by covalent bond breaking and formation, and reverses both the out-of-plane polarization and the in-plane lattice orientation with nonlinear optical polarization. **c,** SHG polarization pattern of a trilayer triangular In_2Se_3 on mica substrate under normal incidence as a function of crystal angle. The three-fold rotational symmetry manifests through the six-fold SHG intensity pattern (black square) when the polarization of the optical excitation and detection are rotated collinearly. Red curve shows the fitting by $I = I_0 \cos^2(3\theta+\theta_0)$, θ is crystal angle. **d,** Out-of-plane dipole probed by angle resolved polarization-selective SHG on the same trilayer sample. Angle-dependent SHG intensity ratio I_p/I_s increases symmetrically with tilted incidence (black triangular) and agrees well with the model of response from out-of-plane dipole to vertical electrical oscillation field, indicating the ratio (13.6:1) between in-plane and out-of-plane second-order susceptibility at 1080 nm pump (red curve, see Supplementary Material section III for model details).

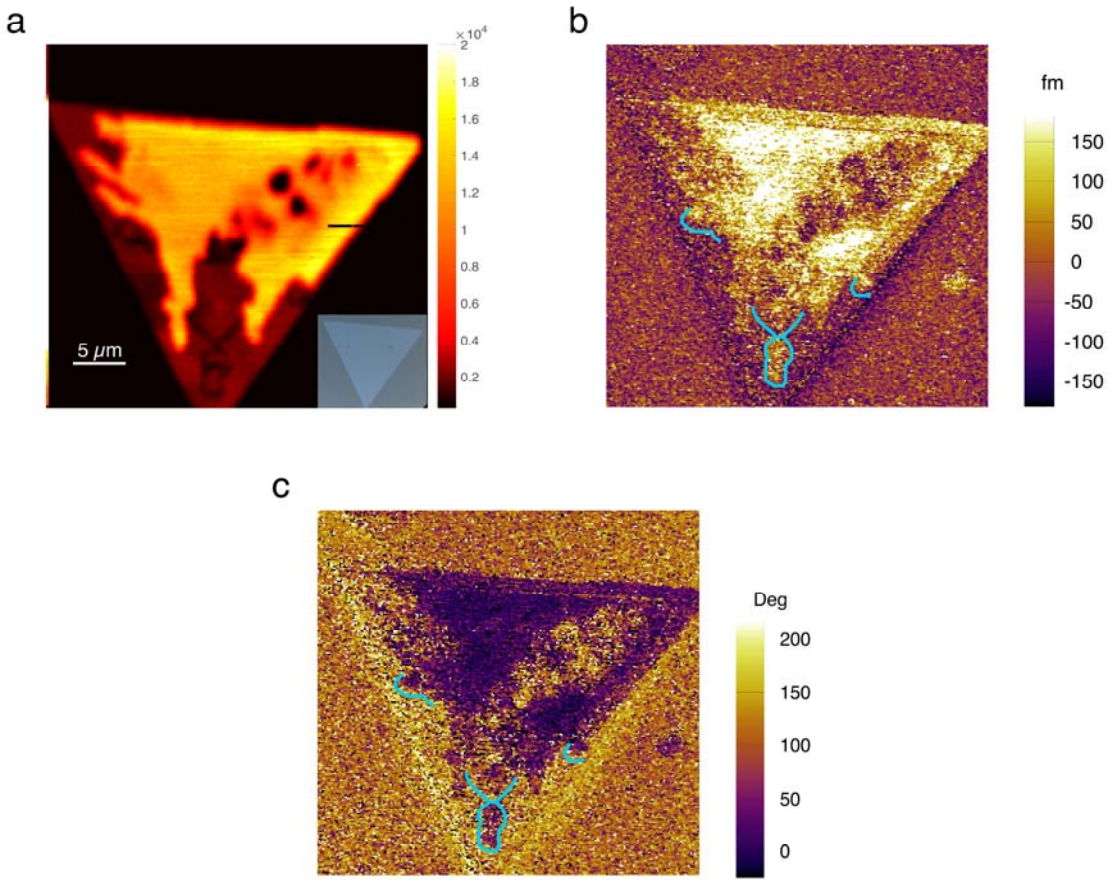

Figure 2| Visualization of domain structure in 2D In_2Se_3 by SHG and piezoresponse mapping. a, SHG mapping of the 3-nm In_2Se_3 crystal, showing intensity contrast in different regions corresponding to domains with different dipole strength that match well with the piezoresponse mapping in **b**. The inset is the optical image of the same sample. SHG intensity dark lines are observed within the region of nearly uniform optical contrast and SHG intensity, that also match the boundaries between domains with 180-degree piezoresponse phase contrast

in **c** (blue curves). They originate from the destructive interference from the oppositely polarized domains.

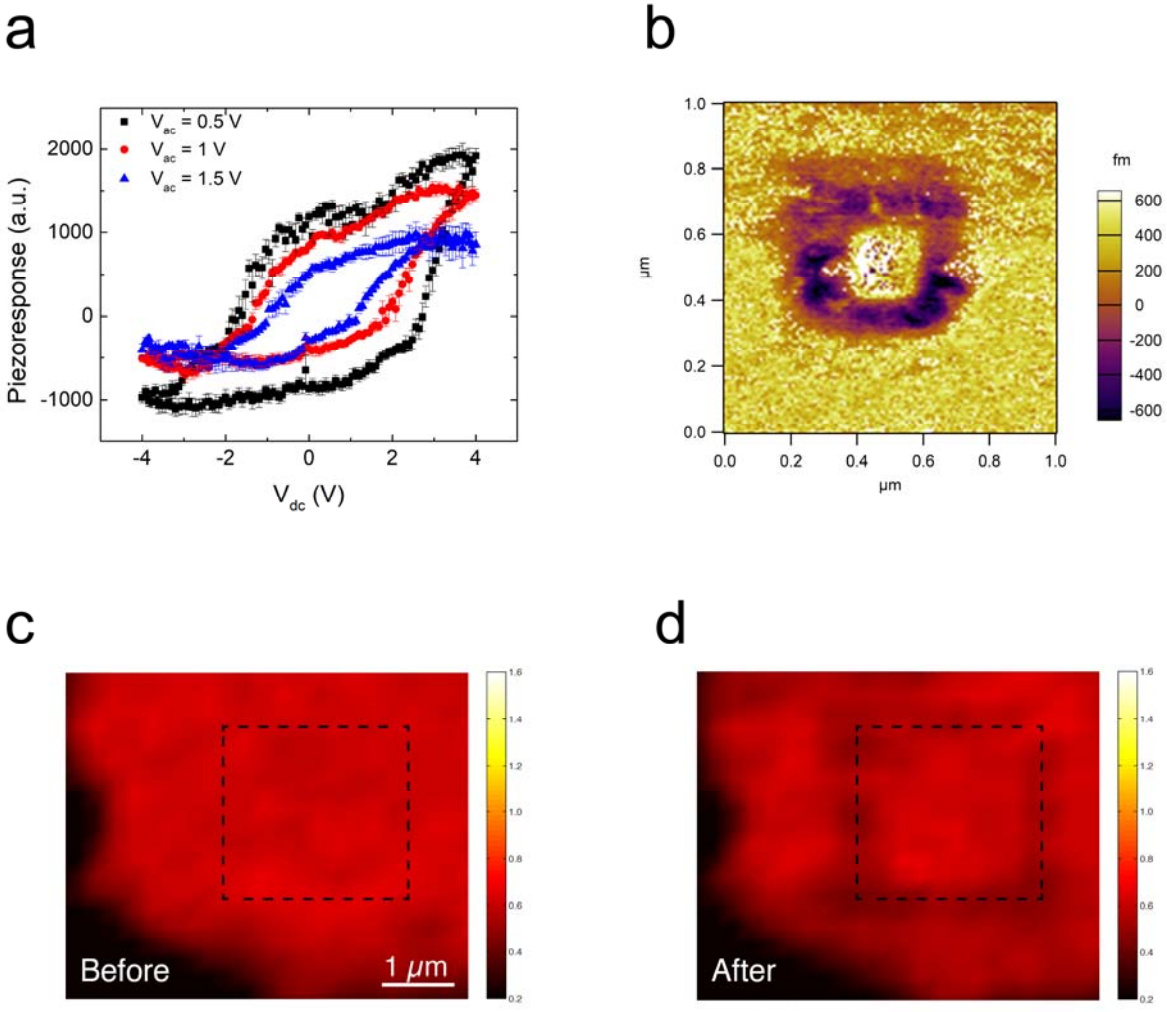

Figure 3 | Electrically switching the out-of-plane ferroelectric polarization and corresponding in-plane atomic configuration through dipole locking. a, The hysteresis of remnant out-of-plane polarization of a 3-nm-thick In_2Se_3 crystal on conductive $SrRuO_3$, as a function of perpendicular poling voltage. Black, red, blue curves represent the normalized piezoresponse measured with Vac = 0.5, 1 and 1.5 V, respectively. The measured coercive voltage is between 2-3 V when V_{ac} is at 0.5V. When V_{ac} progressively increases to 1.5V and approaches the coercive field, both the effective switching voltage and the normalized response signal decrease. The collapse of the hysteresis loop agrees very well with the behavior of the conventional field-switchable ferroelectrics, and is in contrast to the charging artifact of dielectrics. **b,** Polarized domain patterned by electrically biased scanning probe and measured by PFM. The inner box corresponds to positive applied voltage (+6V) and positive piezoresponse while the outer box to negative voltage (-6V) and negative piezoresponse. The piezoresponse signals were obtained from measured resonance amplitude and phase (see Supplementary Material section VII for more details). **c,** SHG intensity mapping on another trilayer In_2Se_3 sample before PFM reversed poling. The area enclosed by dashed line was then scanning by a negatively biased AFM tip. The color bar is in linear scale with arbitrary unit. **d,** SHG mapping after the electrical reversed poling. The written area displays nearly uniform SHG intensity after reversal poling. We observed appearance of SHG dark lines at the boundary of the patterned area resulting from destructive interference between the opposite in-plane crystal orientation and corresponding nonlinear optical polarization inside and outside reversal poling region. This finding not only confirmed the locking between the out-of-plane polarization and in-plane nonlinear optical polarization but demonstrated the functionality to manipulate in-plane crystal orientation through vertical electrical field.

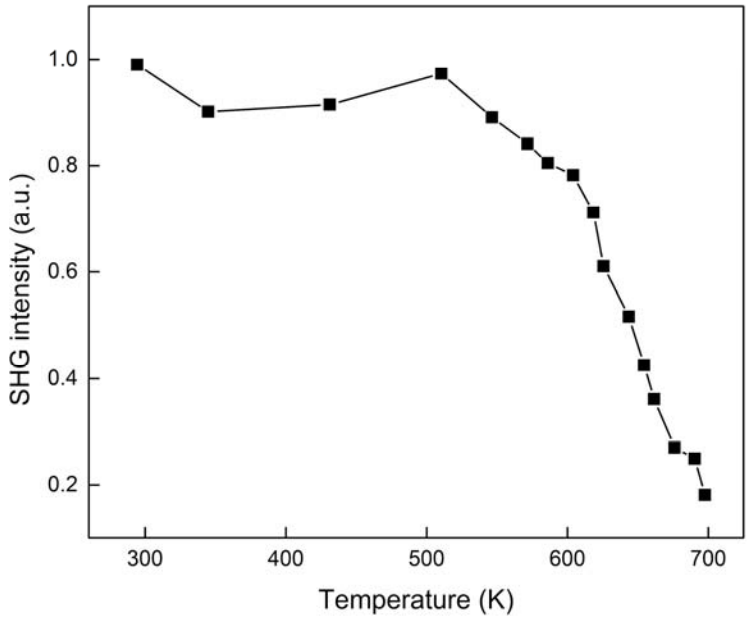

Figure 4 | Observation of temperature-dependent ferroelectric to centrosymmetric phase transition. The SHG intensity and the corresponding ferroelectric ordering remains robust as a four-layer In_2Se_3 sample on SiO_2/Si substrate was heated from room temperature to 600 K. It then dropped sharply to about one sixth of the initial value when the temperature further increased to 700 K, indicating the disappearance of spontaneous polarization and the structural transition to a centrosymmetric phase.